



# Quiet Sun Center to Limb Variation of the Linear Polarization Observed by CLASP2 Across the Mg II *h* and *k* Lines

L. A. Rachmeler<sup>1</sup> , J. Trujillo Bueno<sup>2,3,4</sup> , D. E. McKenzie<sup>5</sup> , R. Ishikawa<sup>6</sup> , F. Auchère<sup>7</sup> , K. Kobayashi<sup>5</sup> , R. Kano<sup>6</sup> , T. J. Okamoto<sup>6</sup> , C. W. Bethge<sup>1,8</sup> , D. Song<sup>6,9</sup> , E. Alsina Ballester<sup>2,3</sup> , L. Belluzzi<sup>10,11,12</sup> , T. del Pino Alemán<sup>2,3</sup> , A. Asensio Ramos<sup>2,3</sup> , M. Yoshida<sup>6,13</sup> , T. Shimizu<sup>14</sup> , A. Winebarger<sup>5</sup> , A. R. Kobelski<sup>5</sup> , G. D. Vigil<sup>5</sup> , B. De Pontieu<sup>15,16,17</sup> , N. Narukage<sup>6</sup> , M. Kubo<sup>6</sup> , T. Sakao<sup>14,18</sup> , H. Hara<sup>6</sup> , Y. Suematsu<sup>6</sup> , J. Štěpán<sup>19</sup> , M. Carlsson<sup>16,17</sup> , and J. Leenaarts<sup>20</sup>

<sup>1</sup> NOAA National Centers for Environmental Information, 325 Broadway, Boulder, CO 80305, USA; [laurel.rachmeler@noaa.gov](mailto:laurel.rachmeler@noaa.gov)

<sup>2</sup> Instituto de Astrofísica de Canarias, E-38205 La Laguna, Tenerife, Spain

<sup>3</sup> Departamento de Astrofísica, Universidad de La Laguna, E-38206 La Laguna, Tenerife, Spain

<sup>4</sup> Consejo Superior de Investigaciones Científicas, Spain

<sup>5</sup> NASA Marshall Space Flight Center, 320 Sparkman Dr. NW, Mail Stop ST13, Huntsville, AL 35805, USA

<sup>6</sup> National Astronomical Observatory of Japan, National Institutes of Natural Science, 2-21-1 Osawa, Mitaka, Tokyo 181-8588, Japan

<sup>7</sup> Institut d'Astrophysique Spatiale, CNRS, Univ. Paris-Sud, Université Paris-Saclay, Bât. 121, F-91405 Orsay, France

<sup>8</sup> Cooperative Institute for Research in Environmental Sciences, 325 Broadway, Boulder, CO 80305, USA

<sup>9</sup> Korea Astronomy and Space Science Institute, 776 Daedeok-daero, Yuseong-gu, Daejeon 34055, Republic of Korea

<sup>10</sup> Istituto Ricerche Solari (IRSOL), Università della Svizzera italiana (USI), CH-6605 Locarno-Monti, Switzerland

<sup>11</sup> Leibniz-Institut für Sonnenphysik (KIS), D-79104 Freiburg, Germany

<sup>12</sup> Euler Institute, Università della Svizzera italiana (USI), CH-6900 Lugano, Switzerland

<sup>13</sup> Department of Astronomical Science, School of Physical Sciences, SOKENDAI (The Graduate University for Advanced Studies), Mitaka, Tokyo 181-8588, Japan

<sup>14</sup> Institute of Space and Astronautical Science, Japan Aerospace Exploration Agency, Sagami-hara, Kanagawa 252-5210, Japan

<sup>15</sup> Lockheed Martin Solar & Astro-physics Laboratory, Palo Alto, CA 94304, USA

<sup>16</sup> Roseland Centre for Solar Physics, University of Oslo, NO-0315 Oslo, Norway

<sup>17</sup> Institute of Theoretical Astrophysics, University of Oslo, NO-0315 Oslo, Norway

<sup>18</sup> Department of Space and Astronautical Science, School of Physical Sciences, SOKENDAI (The Graduate University for Advanced Studies), Sagami-hara, Kanagawa 252-5210, Japan

<sup>19</sup> Astronomical Institute of the Czech Academy of Sciences, Fričova 298, 25165 Ondřejov, Czech Republic

<sup>20</sup> Institute for Solar Physics, Department of Astronomy, Stockholm University, AlbaNova University Centre, SE-106 91, Stockholm, Sweden

Received 2022 May 31; revised 2022 July 5; accepted 2022 July 21; published 2022 August 31

## Abstract

The CLASP2 (Chromospheric LAYer Spectro-Polarimeter 2) sounding rocket mission was launched on 2019 April 11. CLASP2 measured the four Stokes parameters of the Mg II *h* and *k* spectral region around 2800 Å along a 200'' slit at three locations on the solar disk, achieving the first spatially and spectrally resolved observations of the solar polarization in this near-ultraviolet region. The focus of the work presented here is the center-to-limb variation of the linear polarization across these resonance lines, which is produced by the scattering of anisotropic radiation in the solar atmosphere. The linear polarization signals of the Mg II *h* and *k* lines are sensitive to the magnetic field from the low to the upper chromosphere through the Hanle and magneto-optical effects. We compare the observations to theoretical predictions from radiative transfer calculations in unmagnetized semiempirical models, arguing that magnetic fields and horizontal inhomogeneities are needed to explain the observed polarization signals and spatial variations. This comparison is an important step in both validating and refining our understanding of the physical origin of these polarization signatures, and also in paving the way toward future space telescopes for probing the magnetic fields of the solar upper atmosphere via ultraviolet spectropolarimetry.

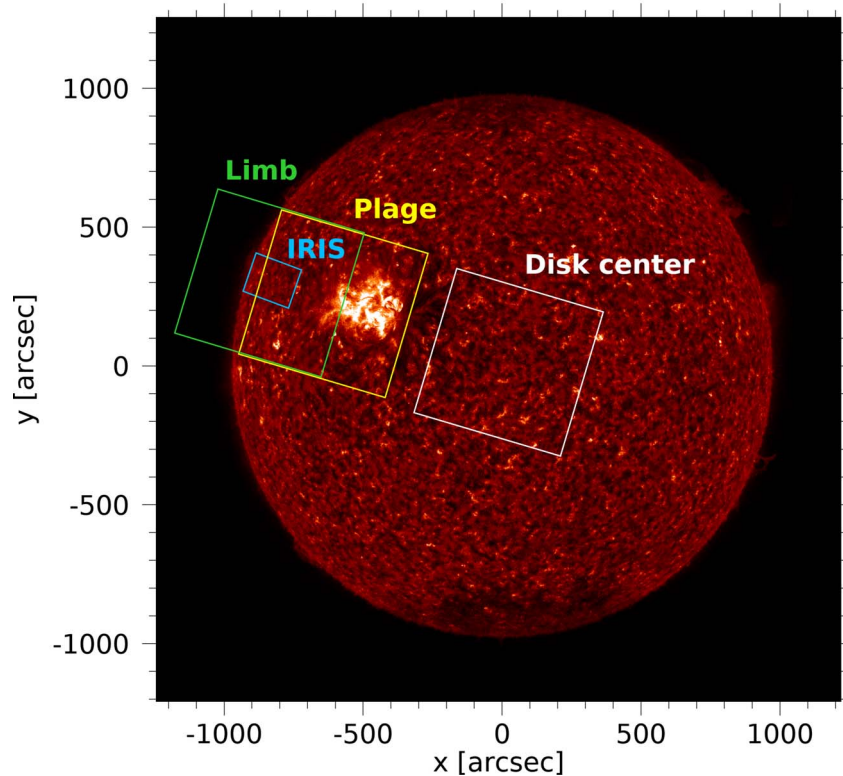
*Unified Astronomy Thesaurus concepts:* [Solar chromosphere \(1479\)](#); [Center to limb observations \(1972\)](#); [Spectropolarimetry \(1973\)](#); [Solar ultraviolet emission \(1533\)](#); [Solar magnetic fields \(1503\)](#); [Quiet solar chromosphere \(1986\)](#)

## 1. Introduction

Our ability to acquire empirical information on the magnetic fields that permeate the atmospheres of the Sun and of other stars largely relies on two key components: the instrumentation needed to measure the polarization of the emitted spectral line radiation, and knowledge gained from theoretical modeling investigations that is required to interpret these spectropolarimetric (SP) observations. The advent of routine monitoring of

solar surface magnetic fields using the polarization produced by the Zeeman effect in photospheric spectral lines catalyzed many new advances in solar physics. It is now a routine matter to estimate the magnetic field throughout the solar atmosphere by combining these photospheric measurements with extrapolation techniques based on simplifying assumptions of force-free fields, which is a reasonable approximation in the solar corona. However, the chromosphere is not a force-free region, and this leads to large errors in the extrapolated field (e.g., De Rosa et al. 2009). Routine measurements of the magnetic field at the base of the corona—or the top of the chromosphere—would significantly improve our ability to accurately model the coronal field and provide key information on the physics of the chromosphere and transition region. This magnetic field is the

AIA 304 Å 2019-04-11T16:54:05



(a) Target Locations

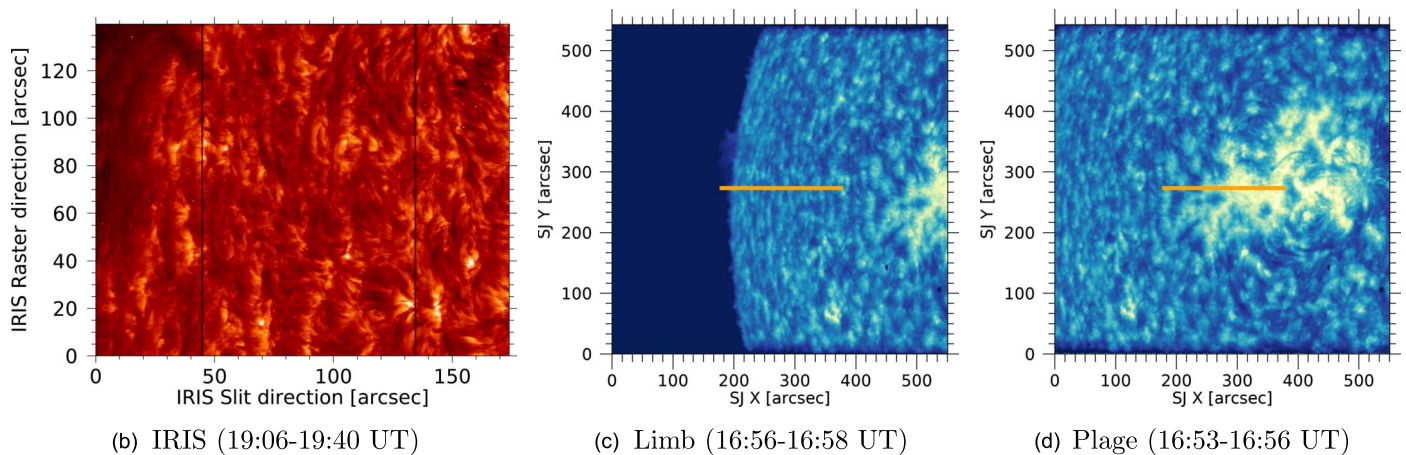


**Figure 1.** (a) The CLASP2 slit-jaw field-of-view locations and the IRIS scan area are indicated for each target superposed on an AIA 304 Å image. (b) IRIS raster of the limb region showing the intensity of the core of the Mg II  $k$  line. The solar limb is to the left of the image. This scan was taken approximately 2 hr after the CLASP flight. (c) CLASP2 slit-jaw Ly $\alpha$  image of the limb target, the slit is highlighted in orange. The solar limb is to the left of the image. (d) CLASP2 slit-jaw Ly $\alpha$  image of the plage target, the slit is highlighted in orange. The solar limb is to the left of the image.

key missing measurement needed to advance our understanding of the solar atmosphere as it drives the mass and energy flow, and dominates the energy budget.

The CLASP (Chromospheric Lyman-Alpha Spectro-Polarimeter, Kobayashi et al. 2012; Kano et al. 2012) and CLASP2 (Chromospheric LAYer Spectro-Polarimeter 2, Narukage et al. 2016; Ishikawa et al. 2021) sounding rocket missions were developed to explore the possibility of mapping the magnetic field in the upper solar chromosphere by providing the first measurements of polarization in prominent ultraviolet (UV) lines. In 2015, the CLASP

instrument measured the linear polarization of the hydrogen Ly $\alpha$  line at 1215.7 Å (Kano et al. 2017) and of the Si III resonance line at 1206.5 Å (Ishikawa et al. 2017) in a quiet region of the solar disk. In 2019, CLASP2 measured the linear and circular polarization of the Mg II  $h$  and  $k$  doublet near 2800 Å in quiet and active regions of the solar disk (Figures 1 and 2). The polarization observed in these lines is due to the combined action of anisotropic radiation pumping and the Hanle and Zeeman effects in the optically thick plasma of the solar chromosphere (for a review, see Trujillo Bueno et al. 2017).

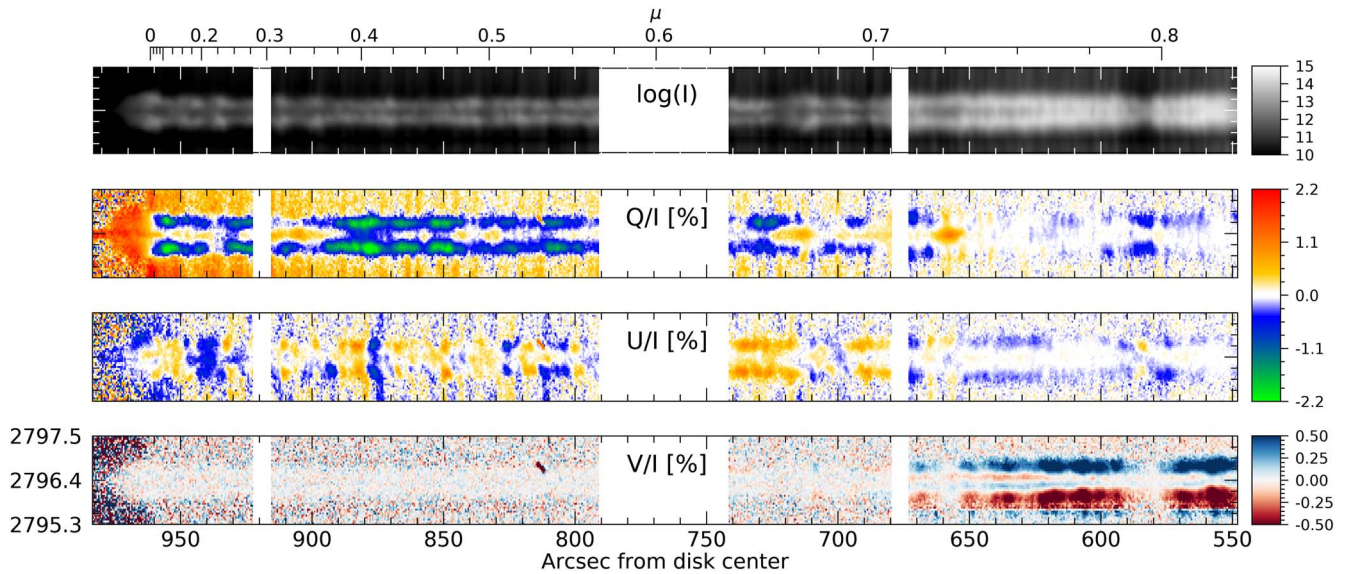


**Figure 2.** Stokes signals of the Mg II  $k$  line for the plage (below 750'', right) and the limb (above 750'', left) pointings. The vacuum wavelengths are labeled in angstroms. The limb of the Sun is on the left side of the figure at  $\mu = 0$ ,  $\mu$  is the cosine of the heliocentric angle. At the limb, the intensity of the light outside of the line cores drops very quickly. The limb location (961'') in the CLASP2 wavelength range was determined by estimating where Stokes  $I$  decreased by  $1/e$  with respect to on-disk near-limb intensity. The reference direction for positive Stokes  $Q$  is parallel to the nearest limb.

Over the last few years, a number of theoretical investigations have enhanced our understanding of the physical mechanisms responsible for the polarization across the Mg II  $h$  and  $k$  lines and its magnetic sensitivity (Belluzzi & Trujillo Bueno 2012; Alsina Ballester et al. 2016; del Pino Alemán et al. 2016, 2020). The linear polarization—Stokes  $Q$  and  $U$ —is controlled by the combined action of scattering processes and the Hanle and magneto-optical effects, while the circular polarization—Stokes  $V$ —is dominated by the Zeeman effect.

In one-dimensional (1D) *unmagnetized* models of the solar atmosphere, the polarization is produced only by the scattering of anisotropic radiation, which produces broad  $Q/I$ <sup>21</sup> profiles with a clear center-to-limb variation (CLV), and  $U/I = 0$  everywhere. The red line in Figure 3 shows this theoretical  $Q/I$  line profile near the limb. At the center of the Mg II  $k$  line  $Q/I > 0$  (Figure 3, (A)), whereas  $Q/I = 0$  at the very center of the (intrinsically unpolarizable)  $h$  line (Figure 3, (C)). The Mg II  $k$  line near wings have negative  $Q/I$  peaks (Figure 3, (B)), with the blue negative peak deeper than the red one, while  $Q/I$  shows an antisymmetric feature in the near wings around the center of the  $h$  line. Such near-wing features are produced by the joint action of partial frequency redistribution (PRD) and quantum-mechanical interference between the substates pertaining to the two upper levels of the Mg II  $h$  and  $k$  lines (hereafter,  $J$ -state interference). The combined action of these physical ingredients is also the cause of the predicted negative  $Q/I$  in the wing wavelengths between the  $h$  and  $k$  lines (Figure 3, (D)), and of the large positive  $Q/I$  values expected for the far blue and red wings of the  $h$  and  $k$  lines (Figure 3, (E)).

In 1D *magnetized* models of the solar atmosphere, the Hanle effect modifies the line-center  $Q/I$  and  $U/I$  signals of the Mg II  $k$  line, while the  $\rho_V Q$  and  $\rho_V U$  magneto-optical terms of the Stokes  $U$  and  $Q$  transfer equations create  $U/I$  wing signals and introduce magnetic sensitivity in the wings of both  $Q/I$  and  $U/I$  (Alsina Ballester et al. 2016; del Pino Alemán et al. 2016, 2020). In contrast to 1D semiempirical static models, the

plasma of the solar atmosphere is dynamic and inhomogeneous in both the horizontal and vertical directions, and the ensuing breaking of the axial symmetry of the incident radiation field at each point within the medium can produce changes in the  $Q/I$  and  $U/I$  line-center and wing signals even in the absence of a magnetic field (e.g., Manso Sainz & Trujillo Bueno 2011; Štěpán & Trujillo Bueno 2016).

Very few observations of the solar Mg II  $h$  and  $k$  polarization exist. A linear polarization data set taken at different times close to the limb at 10 wavelengths in the far wings of the Mg II  $h$  and  $k$  lines was obtained by the Ultraviolet Spectrometer and Polarimeter (UVSP; Woodgate et al. 1980) on board the Solar Maximum Mission (Bohlin et al. 1980). This data set was useful to test the theoretical predictions of Auer et al. (1980) for the linear polarization in the far wings of the lines, namely positive  $Q/I$  signals in the far blue and red wings of the lines and negative  $Q/I$  in the wing between the lines (these predictions were obtained using the approximation of coherent scattering in the observer's frame). The data were initially analyzed by Henze & Stenflo (1987), who found the strong positive  $Q/I$  signals that Auer et al. (1980) had estimated for the far blue and red wings of the  $h$  and  $k$  lines, respectively. Recently, a recalibration of the same limb data has detected the expected negative  $Q/I$  signals between the  $h$  and  $k$  lines (Manso Sainz et al. 2019), the true physical origin of which is the joint action of PRD effects and  $J$ -state interference (Belluzzi & Trujillo Bueno 2012). Before CLASP2, these UVSP data were the only existing observation of the Mg II far-wing polarization, albeit at very low spectral and spatial resolution. The CLASP2 data are the first spectrally and spatially resolved polarization observations of this important line doublet for chromospheric plasma and magnetic field diagnostics; the CLASP2 spatial resolution is less than 2'' and the spectral resolution is 0.1 Å.

The CLASP sounding rocket experiment, the precursor to CLASP2, measured the linear polarization around the hydrogen Ly $\alpha$  line at 1216 Å with the radially oriented spectrograph's slit extending from 20'' off the solar limb to 380'' on the solar disk

<sup>21</sup> As usual, the reference direction for  $+Q$  is parallel to the nearest solar limb.

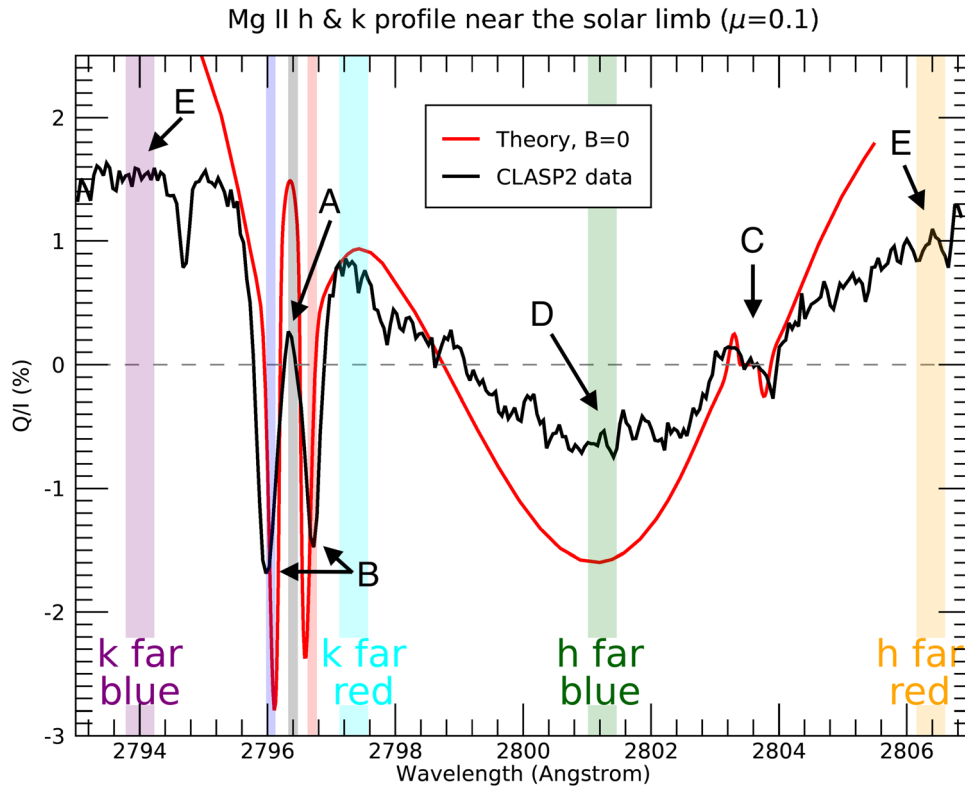


**Figure 3.** Comparison of theoretical (red) and observed (black)  $Q/I$  line profiles near the limb. The observed profile is the average profile for the portion of the slit spanning  $954''.5 < R_{\odot} < 958''.2$  (7 pixels along the slit). The error bar on the black line is less than 0.25%, this error is calculated from  $3\sigma$  photon noise. The theoretical calculation in the  $B = 0$  FAL-C semiempirical model includes the effects of PRD effects and  $J$ -state interference (Belluzzi & Trujillo Bueno 2012). The colors and locations of the shaded regions indicate the wavelength ranges of the data shown in Figures 4 and 5. The capital letter labels correspond to descriptions in the text. The reference direction for positive Stokes  $Q$  is parallel to the nearest limb.

(Kano et al. 2017). CLASP found a clear CLV in the *near wings* of the  $\text{Ly}\alpha$   $Q/I$  profile, in agreement with the theoretical predictions that included PRD effects and  $J$ -state interference (Belluzzi et al. 2012). However, the data did not show any clear CLV at the *center* of the  $\text{Ly}\alpha$   $Q/I$  profile, which is also sensitive to the magnetic field of the chromosphere-corona transition region for fields between approximately 10 and 100 Gauss via the Hanle effect. This lack of CLV in the  $Q/I$  line center contrasts with the clear CLV found there in 1D semiempirical models of the solar chromosphere (Trujillo Bueno et al. 2011) and in a three-dimensional (3D) model of an enhanced network region (Štěpán et al. 2015). Recently, Trujillo Bueno et al. (2018) applied a statistical approach to show that the lack of CLV at the center of the  $\text{Ly}\alpha$   $Q/I$  profile can be reproduced by increasing the geometrical complexity (corrugation of the transition region surface) of the 3D atmospheric model. Other chromospheric lines do show line-center CLV, such as the Ca II K line (Holzreuter & Stenflo 2007), but their line center originates well below the transition region—much deeper than the center of  $\text{Ly}\alpha$ .

The ultimate goal of the CLASP and CLASP2 missions is to obtain UV SP observations to infer the magnetic field in the upper chromosphere. The magnetic field modifies the spectral line polarization, and thus to extract the magnetic information it is important to understand how the polarization is modified by the presence of magnetic fields in different regions of the solar atmosphere. As mentioned above, recent theoretical work has led to significant advances in understanding the predicted polarization in the vicinity of the Mg II  $h$  and  $k$  lines; CLASP2

has provided the first ever data with which to verify these new theoretical advances. We present here the first resolved observations of the CLV of the chromospheric Mg II  $h$  and  $k$  linear polarization and compare these to theoretical predictions of the expected CLV in a semiempirical model of the quiet solar atmosphere. These insights have resulted in a better understanding of the spectral line polarization produced by the solar chromosphere, and are an important part of our efforts toward the goal of measuring the chromospheric magnetic field.

## 2. CLASP2 Instrument, Flight, and Data Reduction

The details of the CLASP2 instrument can be found in Tszuki et al. (2020). CLASP2 reuses most of the hardware from CLASP (Narukage et al. 2015), but there are a few significant changes. The 27 cm aperture Cassegrain telescope feeds into the spectrograph section after the collected light goes through a half-wave plate (for the  $\text{Ly}\alpha$  wavelength, Ishikawa et al. 2013). For CLASP2, the primary mirror of the telescope has been recoated (Yoshida et al. 2018) and the grating completely changed, so that with the same CLASP wave plate, the dual-bandpass spectropolarimeter measures the four Stokes parameters across the Mg II lines, while the slit-jaw imager maintains the same  $\text{Ly}\alpha$  bandpass as in CLASP. A 196'' long slit sits behind a polarization modulation unit (PMU; Ishikawa et al. 2015), which continuously rotates the wave plate. The light that passes through the slit hits the new grating in the spectrograph section, which splits the light into two channels that are fed to two cameras (SP1 and SP2). The individual SP camera polarization analyzers are oriented orthogonal to each

other. The linear polarizers just before the CCD cameras were also changed, and a reimaging optic was also introduced to accommodate the change in wavelength from Ly $\alpha$  to Mg II  $h$  and  $k$  using the same CCD cameras. In CLASP2, the period of the PMU was changed from 4.8 s per rotation to 3.2 s per rotation to accommodate the higher intensity of the Mg II  $h$  and  $k$  lines.

CLASP2 was launched from White Sands Missile Range in New Mexico on 2019 April 11 at 16:51:00 UT and took science-quality data spanning 5 minutes 53 s. During its flight, three solar locations were targeted: the disk center for calibration purposes (15 s, 16:52:52-16:53:07 UT), the edge of a strong-field plage region (156 s, 16:53:40-16:56:16 UT), and the quiet Sun at the limb (141 s 16:56:25-16:58:46 UT). The top panel in Figure 1 shows these locations superposed on a Solar Dynamics Observatory/Atmospheric Imaging Assembly (AIA; Lemen et al. 2012) 304 Å image. The slit is oriented 73°03, 73°0, and 72°8 degrees counterclockwise from solar north in the three pointings respectively, less than 2°5 from radial to where the slit crosses the solar limb. The Interface Region Imaging Spectrograph (IRIS; De Pontieu et al. 2014) also took several co-observation raster scans. Shown in Figure 1b is a large dense 400 step limb context raster that overlays most of the CLASP2 slit (OBS 3620106078). This IRIS Raster time period is (19:06:11-19:40:37 UT), approximately 2 hr after the CLASP2 flight.

This paper focuses on the SP slit data from the second and third targets, the plage and the limb, respectively. All of the data taken at these targets have been calibrated, demodulated, and combined into a single measurement at each target to increase the signal-to-noise ratio. Coordinates were cross-correlated with AIA and IRIS. Calibration performed to the data presented here consists of bias and dark current removal, gain correction, frame transfer smear correction, demodulation, application of the polarization response matrix for crosstalk correction (Song et al. 2022), combining SP1 and SP2, correction of +Q to parallel to the solar limb, and time averaging. The instrumental polarization was confirmed to be negligibly small (Song et al. 2022) using data taken from the first target (disk center). In this paper we only take into account the photon noise as polarization error, which is the dominant error source. For each plot, we indicate the  $3\sigma$  error taking into account averaging in the time, spatial, and spectral directions as appropriate for the plot. The SP data presented here are a combination of both SP cameras. Individual SP images have an exposure time of 200 ms and 16 images are taken during a full PMU rotation period (3.2 s). 47 PMU rotations worth of data were averaged for the plage target and 43 PMU rotations were averaged for the limb target. The calibrated SP data have a spectral plate scale of 0.04988 Å pix<sup>-1</sup> and a spatial plate scale of 0.527 pix<sup>-1</sup>. The resolutions are 0.1 Å and 1.2" respectively (Yoshida et al. 2018; Song et al. 2018).

To extend the range of the CLV beyond a single 196" slit length, we combined the data from the plage and limb targets. The slits are not exactly colinear between those two pointings (see Figure 1a); however, the 4" offset (perpendicular to the slit direction) is small; together the two slits cover 435.5 (0.46R $\odot$ ), with a break of 49.8" between the two pointings. All location coordinates here are presented as a distance from solar disk center. The slit data disk-ward of  $\sim 650''$  sample a strong-field plage region, and these data are not used in the quiet Sun CLV analysis that follows but are shown in the plots

and figures for completeness. The analyses of the circular polarization data in the active region plage are presented in Ishikawa et al. (2021). In this paper we only discuss the CLV in the linear polarization signal because the signal-to-noise ratio of the circular polarization is low outside of the strong-field region as evidenced by the lack of signal in the bottom panel of Figure 2. An overview of the demodulated Mg II  $k$  signal at the plage and limb targets is shown in Figure 2, with the limb near the left edge of the plot at  $\mu = 0$ ;  $\mu$  is the cosine of the heliocentric angle. A piece of dust obscured a small portion ( $\sim 7''$ ) of the slit. The data under the dust have been excluded in this analysis (thin gaps at 675" and 920" in Figure 2).

### 3. Observational Results

Figure 3 shows a comparison of the  $Q/I$  profile observed by CLASP2 near the limb ( $\mu \approx 0.1$ ) with the theoretical  $Q/I$  profile for the *zero field case* obtained by Belluzzi & Trujillo Bueno (2012) in the semiempirical model C of Fontenla et al. (1993; FAL-C model). The theoretical  $Q/I$  profile includes PRD effects and  $J$ -state interference when solving the radiative transfer problem. The combined action of these two physical ingredients results in significant  $Q/I$  signals in the near and far wings of the Mg II  $h$  and  $k$  lines, which become stronger near the limb. As mentioned in Section 1, the presence of a magnetic field and/or the symmetry breaking produced by the horizontal inhomogeneities and macroscopic velocity gradients of the solar chromospheric plasma can have an impact on the  $Q/I$  and  $U/I$  signals, and neither is included in the model results shown in Figure 3. Nevertheless, several key features in the theoretical  $Q/I$  profile corresponding to the unmagnetized FAL-C semiempirical model (hereafter, the  $B = 0$  case) are clearly validated by the CLASP2 data (Figure 3):

- 1 The positive measured Mg II  $k$  line-center signal, which is subject to the Hanle effect depolarization in the presence of a magnetic field (Alsina Ballester et al. 2016; del Pino Alemán et al. 2016, 2020), is weaker in the CLASP2 signal compared to the  $B = 0$  case.
- 2 Negative troughs are measured on either side of the Mg II  $k$  line center (the near wings); the blue wing is more negative than the red wing. The trough–peak–trough nature is caused by PRD effects and this lack of symmetry between the troughs results from the joint action of PRD and  $J$ -state interference (Belluzzi & Trujillo Bueno 2012).
- 3 The Mg II  $h$  line-center observation has zero-polarization with a low-amplitude antisymmetric signal in the near wings. The center of the  $h$  line is intrinsically unpolarizable because the upper and lower levels both have total angular momentum  $J = 1/2$ . The antisymmetric signal is caused by the joint action of PRD and  $J$ -state interference (Belluzzi & Trujillo Bueno 2012).
- 4 A negative trough observed between the Mg II  $h$  and  $k$  centers is also produced by the combined action of PRD and  $J$ -state interference in the  $B = 0$  case (Belluzzi & Trujillo Bueno 2012). The addition of a magnetic field, as in the solar case, would lead to a weaker  $Q/I$  (and give rise to a  $U/I$  signal) in this wavelength range due to magneto-optical effects (Alsina Ballester et al. 2016; del Pino Alemán et al. 2016, 2020) and we see this in the CLASP2 measurement.

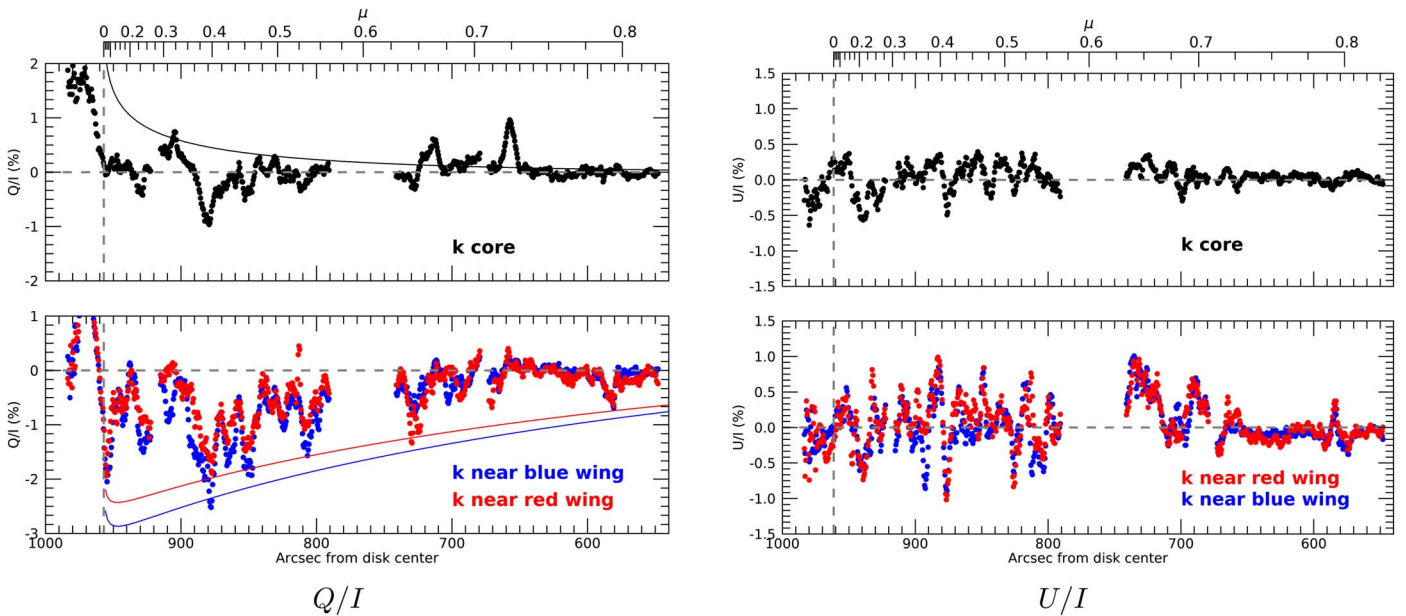


**Figure 4.** Center-to-limb variation of the core and near wings of Mg II  $k$  in  $Q/I$  and  $U/I$  as a function of arcseconds from the disk center and of solar  $\mu$ . The colored dots represent the CLASP2 data and the solid curves the theoretical  $Q/I$  signals calculated in the unmagnetized FAL-C semiempirical model. Note that  $U/I = 0$  in any static one-dimensional unmagnetized model like FAL-C. Dashed lines indicate the location of the limb and zero-polarization. The colors of the dots correspond to the shaded wavelength ranges in Figure 3. The reference direction for positive Stokes  $Q$  is parallel to the nearest limb. The  $3\sigma$  photon noise error on the dots is roughly 0.15% on-disk and 0.6% off-limb.

5 Large positive broadband polarization signals are present on both far edges of the wavelength range, again caused by PRD and  $J$ -state interference (Belluzzi & Trujillo Bueno 2012). Most semiempirical models predict larger  $Q/I$  than was observed by CLASP2 (see Figure 6 in Trujillo Bueno et al. 2017).

The magnetic sensitivity of the  $Q/I$  signal at the center and wings of the lines is dominated by different effects, and the height of the  $\tau = 1$  surface is wavelength dependent. In the far wings, the Mg II radiation samples plasma in the upper photosphere, at an altitude of a few hundred kilometers above the continuum  $\tau = 1$  surface (see Figure 1 of Belluzzi & Trujillo Bueno 2012). In the line center of both  $h$  and  $k$ , the light comes from the upper chromosphere. This wide range of formation heights implies that the polarization across the Mg II  $h$  and  $k$  lines is sensitive to solar magnetic fields from the upper photosphere to close to the chromosphere-corona transition region (see also del Pino Alemán et al. 2020). The challenging task of determining the full stratification of the magnetic field from the intensity and polarization observed across the Mg II resonance lines is out of the scope of this paper. The comparisons of the observed results to the theoretically predicted results for the FAL-C model nonetheless prove important theoretical predictions about the nature of the polarization and the solar chromosphere, and it suggests that the inclusion of magnetic fields in the FAL-C model is needed to explain the lower polarization amplitudes observed by CLASP2.

The linear polarization signal at the Mg II  $k$  line center is modified by the Hanle effect in the presence of upper chromospheric magnetic fields with strengths of approximately 5–100 G (Belluzzi & Trujillo Bueno 2012; Alsina Ballester et al. 2016; del Pino Alemán et al. 2016, 2020). Unlike the very clear CLV of the  $Q/I$  profile at the  $k$  line center calculated in 1D semiempirical models of the solar atmosphere (solid curve

in the top left panel of Figure 4), CLASP2 shows a signal that has strong variations along the slit (dots in Figure 4). Given that the linear polarization at the  $k$  line center is modified by magnetic fields via the Hanle effect, this lack of a clear CLV may indicate that a fluctuating B in the upper chromosphere significantly modifies the CLV predicted by a simple plane parallel model atmosphere. The spatial scale of the fluctuation of Stokes  $I$  along the slit is on the order of  $10''$ , consistent with network/internetwork spacing that would correspond with field changes. However, the solar chromosphere is highly inhomogeneous and dynamic; the magnetic field is not the only cause of symmetry breaking capable of modifying the scattering line polarization. CLASP also did not observe any clear CLV at the Ly $\alpha$  line center, which was shown to be consistent with 3D model atmospheres having a highly corrugated transition region surface (Trujillo Bueno et al. 2018).

The Mg II  $k$  blue and red near wings of the  $Q/I$  profile show a clear CLV between about  $690''$  and  $890''$ , though this trend does not appear to continue to the limb (lower left panel of Figure 4). Via the magneto-optical effects, these near-wing signals are sensitive to the depolarizing effect caused by the presence of magnetic fields in the lower solar chromosphere, with strengths similar to those that produce the Hanle effect at the  $k$  line center. This explanation would be consistent with the observations. The theoretical CLV calculated in the unmagnetized FAL-C semiempirical model of the quiet Sun (the solid curves in the same figure panel) generally have a stronger polarization signature than the CLASP2 measurements.

The center of the neighboring Mg II  $h$  line is intrinsically unpolarizable and the distinctive antisymmetric  $Q/I$  signal observed around the line center is only obtained in theoretical calculations that include both PRD effects and  $J$ -state interference (Belluzzi & Trujillo Bueno 2012).

As expected, all  $U/I$  signals of the Mg II  $k$  line (both at the center and at the near wings) fluctuate around zero, without any CLV (right panels of Figure 4). The corresponding  $Q/I$  signals

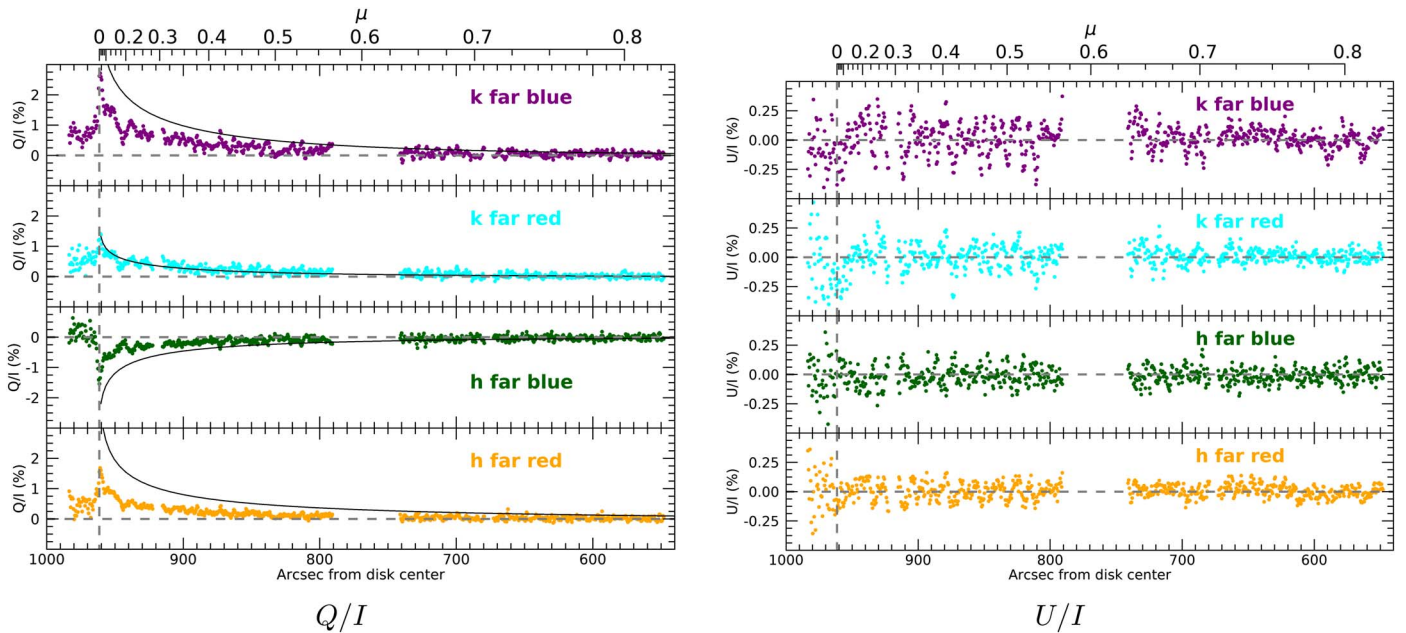


**Figure 5.** Center-to-limb variation of the far wings of Mg II  $h$  and  $k$  in  $Q/I$  and  $U/I$  as a function of arcseconds from the disk center and solar  $\mu$ , with the colored dots showing the CLASP2 data and the solid curves the theoretical  $Q/I$  signals calculated in the unmagnetized FAL-C semiempirical model. Note that  $U/I = 0$  in any static one-dimensional unmagnetized model like FAL-C. Dashed lines indicate the location of the limb and zero-polarization. The colors of the dots correspond to the shaded wavelength ranges in Figure 3. The reference direction for positive Stokes  $Q$  is parallel to the nearest limb. The  $3\sigma$  photon noise error on the dots is roughly 0.14% on-disk and 0.6% off-limb.

also fluctuate along the spatial direction of the radially oriented slit (left panels), but the wing signals do not fluctuate around zero. These  $Q/I$  and  $U/I$  spatial fluctuations are likely caused by the local symmetry breaking due to the 3D nature of the solar chromosphere, but the amplitudes of the fluctuations themselves appear to be sensitive to the magnetic field strength—note that these polarization amplitudes are damped inside the plage region disk-ward of  $650''$ , where the magnetic field is stronger. As mentioned above, the Hanle effect (which operates at the  $k$  line center) and the magneto-optical effects (which operate in the near and far wings all across the Mg II doublet) tend to significantly reduce the scattering polarization amplitudes. This occurs mainly for magnetic fields with strengths at or above  $0.2B_H$ , where  $B_H = 22$  G is the critical Hanle field strange for the  $k$  line (Alsina Ballester et al. 2016; del Pino Alemán et al. 2016, 2020).

Although this was not explicitly included in the theoretical paper by Belluzzi & Trujillo Bueno (2012), another result from their calculations with the FAL-C semiempirical model is that the far wings of the lines have a clear CLV in  $Q/I$ ; the solid black curves in the left panels of Figure 5 show the CLV at the four far-wing wavelength bands. The dots in the same panels show the CLV observed by CLASP2 at these wavelengths. Interestingly, while the observed and calculated CLV match in the  $k$  far red wavelength, the amplitudes of the observed CLV in the other far-wing wavelengths are smaller than the theoretical ones. As shown by del Pino Alemán et al. (2016, 2020) magneto-optical effects introduce magnetic sensitivity in the far wings of the Mg II  $h$  and  $k$  lines, depolarizing the  $Q/I$  wing signals for magnetic fields as weak as 22 G. These far  $Q/I$  wing signals originate in the upper photosphere, and we interpret the smaller amplitudes of the observed CLV curves as due to magneto-optical depolarization by the magnetic fields of the upper solar photosphere.

The  $U/I$  far-wing signals fluctuate around zero (right panels of Figure 5), which is mostly as expected. As stated earlier, theoretical models predict that when a magnetic field is present, the magneto-optical effects can transfer signal from Stokes  $Q$  to Stokes  $U$  in the far wings (Alsina Ballester et al. 2016; del Pino Alemán et al. 2016, 2020). The effect increases when the longitudinal component of the magnetic field is stronger and when  $Q$  is greater, such as very close to the limb where the  $Q/I$  wing signal rises according to its CLV. The amplitude of the  $U/I$  signals very near the limb ( $0 < \mu < 0.2$ ) in the far wings may thus show a CLV due to these magneto-optical effects (Figure 5, right), but the observations are not conclusive. More work is in progress to explore this possibility.

#### 4. Discussion

We have presented the first ever spectrally resolved measurements of the linear polarization across the Mg II  $h$  and  $k$  lines of the solar chromosphere, with a spatial resolution of less than  $2''$ . These unprecedented measurements provide unique data to confirm or refute our current theoretical understanding of the physical mechanisms that control the polarization of these strong UV lines, which encode important information on the magnetism of the solar chromosphere. The focus of this paper is the linear polarization observed by CLASP2 in the quiet Sun, with emphasis on the CLV.

The key findings are summarized as follows:

1. The overall shape of the  $Q/I$  polarization signal is consistent with theoretical predictions when PRD and  $J$ -state interference are included in the radiative transfer calculations (Belluzzi & Trujillo Bueno 2012), proving the importance of both of these effects for the Mg II resonance lines (Figure 3).
2. Although no clear CLV is seen at the  $Q/I$  line center of Mg II  $k$  (Figure 4, upper left panel), the observed line-center signal does not fluctuate around the zero-

polarization level as clearly as CLASP measured for the Ly $\alpha$   $Q/I$  line-center signal (Kano et al. 2017). The center of the hydrogen Ly $\alpha$  line originates very close to the corrugated surface that delineates the chromosphere-corona transition region, and the observational fact that the CLV of its  $Q/I$  line-center signal fluctuates around zero could be explained in terms of the geometrical complexity of such transition region layer (Trujillo Bueno et al. 2018). The Mg II  $k$  line-center  $Q/I$  patterns observed by CLASP2 could indicate that both magnetic field variations and corrugation of the originating surface contribute to the observation.

3. CLV is found in the near wings of Mg II  $k$  in  $Q/I$  (Figure 4, lower left panel). The CLV is clearly inferred disk-ward of  $\mu = 0.4$ , but there is a break in the pattern closer to the limb. Depolarization by magneto-optical effects produced by chromospheric magnetic fields could be responsible for the disparity between the model and observations, but more theoretical work is needed to be able to model the linear polarization in the wings of strong resonance lines taking into account the combined action of magneto-optical effects and the symmetry breaking caused by horizontal atmospheric inhomogeneities.
4. The predicted antisymmetric  $Q/I$  signal around the Mg II  $h$  line center was validated (Figure 3, C). This very distinctive signal is only seen in the theoretical models when both PRD and  $J$ -state interference are included (Belluzzi & Trujillo Bueno 2012).
5. The broadband  $Q/I$  CLV trends in the far wings of Mg II  $h$  and  $k$  (Figure 5, left panels) are consistent with theoretical calculations when PRD effects,  $J$ -state interference, and magneto-optical effects are accounted for (del Pino Alemán et al. 2016, 2020; Alsina Ballester et al. 2016).

More work is needed to fully understand these new observations. Nevertheless, the comparison of the unique data provided by CLASP2 with the theoretical results from the 1D radiative transfer investigations carried out over the last few years (Belluzzi & Trujillo Bueno 2012; Alsina Ballester et al. 2016; del Pino Alemán et al. 2016, 2020) clearly shows that we have a good physical understanding of the mechanisms that control the linear polarization across the Mg II  $h$  and  $k$  lines. Additionally, a previously published CLASP2 investigation showed the usefulness of the circular polarization signals in the observed CLASP2 wavelength region by calculating the line-of-sight magnetic field strength at multiple heights using the Mg II doublet and other UV lines in an active region plage (Ishikawa et al. 2021).

The next challenge on the theoretical front will be to solve the 3D radiative transfer problem taking into account the PRD effects and  $J$ -state interference. Regarding observations, it is clear that routine SP observations of this sort would result in rich scientific information about the magnetic field that would benefit a broad solar community, and so we strongly advocate for a solar space telescope equipped with a CLASP-like spectropolarimeter for probing the upper solar chromosphere.

CLASP2 is an international partnership between NASA/MSFC, NAOJ, JAXA, IAC, and IAS; additional partners include ASCR, IRSOL, LMSAL, and the University of Oslo. The CLASP2 team acknowledges S. Ishikawa, who led the development of the critical component of the polarization modulation unit (PMU) at ISAS/JAXA. The Japanese participation was funded

by ISAS/JAXA as a Small Mission-of-Opportunity Program, JSPS KAKENHI grant Nos. JP25220703 and JP16H03963, 2015 ISAS grant for Promoting International Mission Collaboration, and by 2016 NAOJ grant for Development Collaboration. The USA participation was funded by NASA Award 16-HTIDS16\_2-0027. The Spanish participation was funded by the European Research Council (ERC) under the European Union's Horizon 2020 research and innovation program (Advanced grant agreement No. 742265). The French hardware participation was funded by CNES funds CLASP2-13616A and 13617A. L.B. acknowledges the funding received through SNSF grants 200021-175997 and CRSII5-180238. B.D.P. was supported by NASA Contract NNG09FA40C (IRIS).

## ORCID iDs

L. A. Rachmeler  <https://orcid.org/0000-0002-3770-009X>  
 J. Trujillo Bueno  <https://orcid.org/0000-0001-5131-4139>  
 D. E. McKenzie  <https://orcid.org/0000-0002-9921-7757>  
 R. Ishikawa  <https://orcid.org/0000-0001-8830-0769>  
 F. Auchère  <https://orcid.org/0000-0003-0972-7022>  
 K. Kobayashi  <https://orcid.org/0000-0003-1057-7113>  
 R. Kano  <https://orcid.org/0000-0002-2093-085X>  
 T. J. Okamoto  <https://orcid.org/0000-0003-3765-1774>  
 C. W. Bethge  <https://orcid.org/0000-0001-9076-6461>  
 D. Song  <https://orcid.org/0000-0003-3034-8406>  
 E. Alsina Ballester  <https://orcid.org/0000-0001-9095-9685>  
 L. Belluzzi  <https://orcid.org/0000-0002-8775-0132>  
 T. del Pino Alemán  <https://orcid.org/0000-0003-1465-5692>  
 A. Asensio Ramos  <https://orcid.org/0000-0002-1248-0553>  
 M. Yoshida  <https://orcid.org/0000-0003-4088-7673>  
 A. Winebarger  <https://orcid.org/0000-0002-5608-531X>  
 A. R. Kobelski  <https://orcid.org/0000-0002-4691-1729>  
 G. D. Vigil  <https://orcid.org/0000-0002-7219-1526>  
 B. De Pontieu  <https://orcid.org/0000-0002-8370-952X>  
 N. Narukage  <https://orcid.org/0000-0002-6330-3944>  
 M. Kubo  <https://orcid.org/0000-0001-5616-2808>  
 T. Sakao  <https://orcid.org/0000-0003-2991-4159>  
 H. Hara  <https://orcid.org/0000-0001-5686-3081>  
 Y. Suematsu  <https://orcid.org/0000-0003-4452-858X>  
 J. Štěpán  <https://orcid.org/0000-0002-8292-2636>  
 M. Carlsson  <https://orcid.org/0000-0001-9218-3139>  
 J. Leenaarts  <https://orcid.org/0000-0003-4936-4211>

## References

- Alsina Ballester, E., Belluzzi, L., & Trujillo Bueno, J. 2016, *ApJL*, 831, L15  
 Auer, L. H., Rees, D. E., & Stenflo, J. O. 1980, *A&A*, 88, 302  
 Belluzzi, L., & Trujillo Bueno, J. 2012, *ApJL*, 750, L11  
 Belluzzi, L., Trujillo Bueno, J., & Štěpán, J. 2012, *ApJL*, 755, L2  
 Bohlin, J. D., Frost, K. J., Burr, P. T., Guha, A. K., & Withbroe, G. L. 1980, *SoPh*, 65, 5  
 De Pontieu, B., Title, A. M., Lemen, J. R., et al. 2014, *SoPh*, 289, 2733  
 De Rosa, M. L., Schrijver, C. J., Barnes, G., et al. 2009, *ApJ*, 696, 1780  
 del Pino Alemán, T., Casini, R., & Manso Sainz, R. 2016, *ApJL*, 830, L24  
 del Pino Alemán, T., Trujillo Bueno, J., Casini, R., & Manso Sainz, R. 2020, *ApJ*, 891, 91  
 Fontenla, J. M., Avrett, E. H., & Loeser, R. 1993, *ApJ*, 406, 319  
 Henze, W., & Stenflo, J. O. 1987, *SoPh*, 111, 243  
 Holzreuter, R., & Stenflo, J. O. 2007, *A&A*, 472, 919  
 Ishikawa, R., Kano, R., Bando, T., et al. 2013, *ApOpt*, 52, 8205  
 Ishikawa, R., Trujillo Bueno, J., del Pino Alemán, T., et al. 2021, *SciA*, 7, eabe8406  
 Ishikawa, R., Trujillo Bueno, J., Uitenbroek, H., et al. 2017, *ApJ*, 841, 31  
 Ishikawa, S., Shimizu, T., Kano, R., et al. 2015, *SoPh*, 290, 3081  
 Kano, R., Bando, T., Narukage, N., et al. 2012, *Proc. SPIE*, 8443, 84434F  
 Kano, R., Trujillo Bueno, J., Winebarger, A., et al. 2017, *ApJL*, 839, L10

- Kobayashi, K., Kano, R., Trujillo-Bueno, J., et al. 2012, in ASP Conf. Ser. 456, Fifth Hinode Science Meeting, ed. L. Golub, I. De Moortel, & T. Shimizu (San Francisco, CA: ASP), 233
- Lemen, J. R., Title, A. M., Akin, D. J., et al. 2012, *SoPh*, 275, 17
- Manso Sainz, R., del Pino Alemán, T., Casini, R., & McIntosh, S. 2019, *ApJL*, 883, L30
- Manso Sainz, R., & Trujillo Bueno, J. 2011, *ApJ*, 743, 12
- Narukage, N., Auchère, F., Ishikawa, R., et al. 2015, *ApOpt*, 54, 2080
- Narukage, N., McKenzie, D. E., Ishikawa, R., et al. 2016, *Proc. SPIE*, 9905, 990508
- Song, D., Ishikawa, R., Kano, R., et al. 2018, *Proc. SPIE*, 10699, 106992W
- Song, D., Ishikawa, R., Kano, R., et al. 2022, *SoPh*, submitted
- Trujillo Bueno, J., Landi Degl’Innocenti, E., & Belluzzi, L. 2017, *SSRv*, 210, 183
- Trujillo Bueno, J., Štěpán, J., Belluzzi, L., et al. 2018, *ApJL*, 866, L15
- Trujillo Bueno, J., Štěpán, J., & Casini, R. 2011, *ApJL*, 738, L11
- Tsuzuki, T., Ishikawa, R., Kano, R., et al. 2020, *Proc. SPIE*, 11444, 114446W
- Štěpán, J., & Trujillo Bueno, J. 2016, *ApJL*, 826, L10
- Štěpán, J., Trujillo Bueno, J., Leenaarts, J., & Carlsson, M. 2015, *ApJ*, 803, 65
- Woodgate, B. E., Tandberg-Hanssen, E. A., Bruner, E. C., et al. 1980, *SoPh*, 65, 73
- Yoshida, M., Song, D., Ishikawa, R., et al. 2018, *Proc. SPIE*, 10699, 1069930